Astron. Astrophys. 330, 253–264 (1998)

ASTRONOMY
AND
ASTROPHYSICS

Inference of steady stellar wind $v(r)$ laws from optically thin emission lines

II. Occultation effects and the determination of intrinsic stellar properties

R. Ignace[1], **J.C. Brown**[1], **L.L. Richardson**[1], **and J.P. Cassinelli**[2]

[1] Department of Physics and Astronomy, University of Glasgow, Glasgow, G12 8QQ, UK
[2] Department of Astronomy, University of Wisconsin, Madison, WI 53706-1582, USA

Received 8 July 1997 / Accepted 23 September 1997

Abstract. This paper extends previous work on the inversion of line profiles to obtain wind velocity laws to a case that includes the occultation of light from the far side of the star. The velocity law $v(r)$ is assumed to be from a wind that is steady and spherically symmetric. The wind is also assumed to be optically thin in the emission line profile. The major result here is the derivation of an *analytic* inversion formula. The effects of stellar occultation are shown to produce a significant change in the analysis from paper I, and by accounting for the occultation, the red-shifted emission of P Cygni profiles can be used to obtain $v(r)$. Using simulated line profiles as generated from a radiation transport code to test the procedure, the inversion technique based on optically thin lines successfully recovers $v(r)$ distributions for weak LTE H_α profiles from hot star winds. Even in the case of NLTE H_α lines, the technique is seen to reproduce the model velocity distribution quite well. Our inversion technique thus remains robust outside the scope of our assumptions, owing primarily to an empirical approach for applying the method. An important aspect of our empirical approach is the possibility of estimating intrinsic stellar and wind properties, such as the mass-loss rate $\dot{M}$, photospheric radius R, and the stellar distance D. As an example, photospheric stellar radii are derived from the model profiles and found to be in good agreement with the input values, with typical errors of about 5%. Even in the NLTE case, the photospheric radii are underestimated by only 10–20%.

Key words: line: profiles – stars: early-type – stars: fundamental parameters – stars: mass-loss

1. Introduction

The distribution of wind speed v as a function of radius r is an important property of a stellar wind, because the velocity law relates to the mechanisms that accelerate the flow. Information about the velocity law is present in the profiles of lines that are formed in the wind. In the first half of this century, Beals (1929) and Menzel (1929) interpreted the highly broadened lines (500–3000 km s^{-1}) lines of novae and Wolf-Rayet stars as arising from mass-loss. Chandrasekhar (1934) investigated the line profiles (or "contours") that might result from stellar mass-loss under a variety of assumptions concerning the outflow properties. Since that time, wind broadened line profiles have been modelled in one of two ways: (a) assume the velocity distribution to be known and allow parameters such as the mass-loss rate, ionization fraction, etc to vary or (b) take the velocity distribution $v(r)$ as unknown yet parametrized according to theoretical expectations and determine the parameters governing the velocity law from a best fit to the line profile. Thus, there are currently no reliable or straightforward procedures of extracting the information content in the profiles to retrieve the wind velocity structure directly without making some assumptions about the form of $v(r)$.

A significant literature exists for this forward analysis problem, where $v(r)$ is prescribed, usually based on the β-law distribution predicted by radiation line driven wind theory (c.f., Lucy & Solomon 1970; Castor et al. 1975; Friend & Abbott 1986; Pauldrach et al. 1986). Numerous authors have sought to derive stellar parameters from the line profile fitting of resonance lines (e.g., Lamers et al. 1987; Groenewegen & Lamers 1989) and recombination lines (Puls et al. 1996), and also from matching observed line equivalent widths (Leitherer 1988; Lamers & Leitherer 1993).

In this series of papers (this being the second), we explore the use of optically thin emission lines for deriving directly the velocity distribution $v(r)$ (and hence density) of steady spherical stellar winds from line profile inversion without resorting to any specified parametrization. The inversion approach has the disadvantage of requiring some simplifying assumptions to make the problem tractable, but in the cases where the simplifications (see below) are justifiable, the results of the inversion can provide valuable information for independently testing current

Send offprint requests to: R. Ignace

parametrizations of $v(r)$ and guiding their selection in analyses where our assumptions no longer apply.

In Paper I (Brown et al. 1997; hereafter BRCI), an integral inversion method was developed whereby a monotonic velocity structure $v(r)$ in a spherical wind could be derived from the profile $F_\lambda(\Delta\lambda)$ of an optically thin emission line of rest wavelength λ_0. In that analysis emphasis was given to the red wing of $F_\lambda(\Delta\lambda)$, so that absorption of starlight by the wind could be ignored. However, the occultation of wind emission from behind the star was also ignored, which can have substantial effects on the profile shape of the red wing. For example, considerations of a recombination line formed in a constant expansion wind reveals that the total line emission is reduced by approximately 11% owing to stellar occultation. Hence, the effect of occultation must be addressed if accurate $v(r)$ distributions are to be derived from the line profile inversions.

In Sect. 2, the effects of occultation are incorporated into the inversion technique of BRCI. Applications to synthetic profiles are presented and discussed in Sect. 3. We further consider the potential for deriving fundamental stellar and wind parameters in Sect. 4. A discussion of these results and future pursuits of inversion methods for deriving stellar wind structures are given in Sect. 5. In particular, the inversion technique described here can be applied to winds that are either optically thin *or* thick in the continuum (e.g., the Wolf-Rayet stars). Lastly, the Appendix details the profile inversion of resonance line profiles, in contrast to the recombination lines considered in BRCI.

2. Recovery of wind velocity laws in the case of occultation

In this section the formalism of BRCI is briefly reviewed, and the consequences of neglecting occultation are illustrated. The inversion technique for deriving wind velocity distributions is then expanded to include the effects of occultation.

2.1. The effects of occultation

Following BRCI for an optically thin spherical wind ignoring both occultation and absorption, the flux of line emission produced by a stellar wind is

$$F_\lambda(\Delta\lambda) = \frac{c}{2\lambda_0 D^2} \int_{r_{\rm min}}^{\infty} \frac{j(r)\, r^2}{v(r)}\, dr, \tag{1}$$

where $r_{\rm min}$ is the radius in the wind where $\Delta\lambda = \lambda_0 v(r_{\rm min})/c$, and D is the distance to the star.

For a recombination line formed in an isothermal wind, the emissivity is $j(r) = f_0(T)\, n_{\rm e}^2$ (Wm^{-3}), where the temperature dependent function f_0 equals hc/λ_0 times the recombination coefficient for the line. Substituting into Eq. (1) gives

$$F_\lambda(\tilde{w}) = \frac{1}{4\,\alpha} \int_{x_{\rm min}(\tilde{w})}^{\infty} \frac{dx}{x^2\, w^3(x)}, \tag{2}$$

where the normalized variables $x = r/R$, $w(x) = v(r)/v_\infty$, and $\tilde{w} = c\Delta\lambda/v_\infty\lambda_0$ is the normalized velocity Doppler shift in the profile from line center. At $x = x_{\rm min}$, $\tilde{w}$ is equal to $w(x_{\rm min})$. The parameter α is

$$\alpha = \frac{8\pi^2\, D^2\, \lambda_0\, m_{\rm H}^2\, R\, v_\infty^3}{f_0(T)\, \dot{M}_{\rm e}^2\, c}, \tag{3}$$

where we have defined the shorthand $\dot{M}_{\rm e} = \dot{M}/\mu_{\rm e}$, because the mass-loss rate $\dot{M}$ and mean molecular weight per free electron $\mu_{\rm e}$ always appear in the ratio. Implicit in Eqs. (2) and (3) is the assumption of a constant departure coefficient for whatever line is being considered. These expressions could be modified to include a radius dependent departure coefficient, and even a temperature distribution, but such additional complexities would not allow a direct analytic solution to the inversion problem of a single profile. Later, it will be shown that for mildly NLTE lines, the profile inversion does reasonably well in recovering the wind $v(r)$.

It is convenient to introduce the continuum normalized profile. Denoting by $F_{\rm c}$ the continuum flux at line center (assumed constant over the width of the line), then

$$\Phi(\tilde{w}) = \frac{F_{\rm c} + F_\lambda(\tilde{w})}{F_{\rm c}} = 1 + \frac{1}{4\alpha F_{\rm c}} \int_{x_{\rm min}(\tilde{w})}^{\infty} \frac{dx}{x^2\, w^3(x)}, \tag{4}$$

The introduction of Φ is a slight departure from the formulation used in BRCI, but rectified profiles are a common way of displaying and discussing spectral lines in the literature.

It was shown by BRCI that the wind velocity could be recovered from an optically thin emission line profile by inverting Eq. (4). The relation of the wind velocity distribution to the line profile is given (with $y = 1/x = R/r$) by

$$y(w) = \alpha\, F_{\rm c} \int_{w^4}^{1} \left(-\frac{d\Phi}{d\tilde{w}}\right) d\tilde{w}^4, \tag{5}$$

where $d\Phi/d\tilde{w} = (\lambda_0 v_\infty/c)\, d\Phi/d\Delta\lambda$ represents the slope of the emission line profile with respect to the observed Doppler shift. Recall that for an optically thin line, a spherical shell expanding at constant speed will produce an elementary rectangular emission profile that has a half width equal to the expansion speed. It follows, therefore, that a spherical wind with a radially varying velocity distribution consists of a superposition of rectangular profiles, each of which may be associated with a thin shell of approximately constant expansion velocity. Now since the emission of any given shell is proportional to the square of the density in that shell, the slope information contained in the observed emission line profile relates to the actual wind velocity distribution. However, Eq. (5) is only valid for the blue-shifted emission if absorption may be neglected or for the red-shifted emission if occultation may be neglected, of which neither condition is likely to be realized. Hence, a modification of Eq. (5) is required to recover the wind velocity law in more realistic situations.

Before presenting a solution to the case of occultation, a simple example is considered to illustrate the rather dramatic consequences that the neglect of occultation effects can have on the inferred velocity distribution. It has already been pointed out

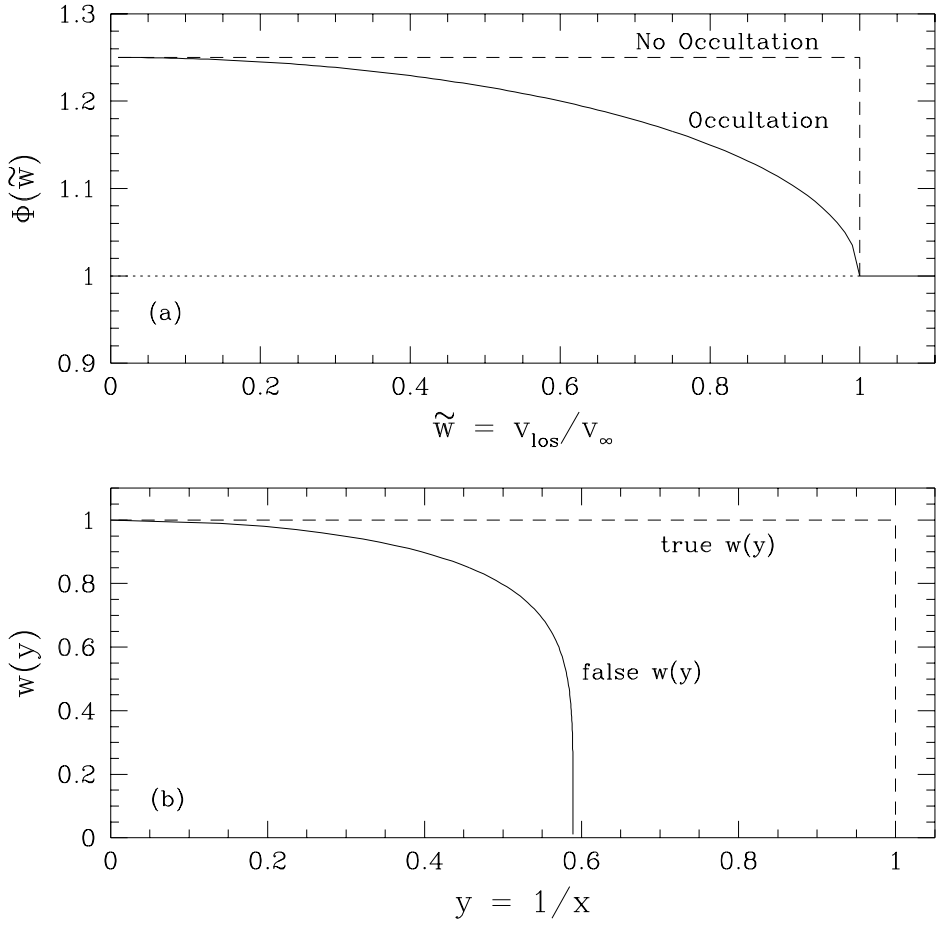

Fig. 1. The redshifted emission line profile plotted against the normalized line-of-sight velocity $v_{\rm los}$ for a spherical and constant expansion wind (top) and the inferred wind velocity when occultation is neglected (bottom)

that a spherical shell with constant expansion speed will yield a rectangular profile when occultation is ignored. In the case of occultation, the profile is not in fact rectangular for a wind expanding at constant speed $w = 1$. With $x_{\rm min} = (1 - \tilde{w}^2)^{-1/2}$ to take occultation into account, it can be shown from Eq. (2) that the line profile has the simple form

$$\Phi = 1 + \frac{1}{4\alpha F_{\rm c}} \sqrt{1 - \tilde{w}^2}, \tag{6}$$

which is valid for $\tilde{w} \geq 0$. Setting $\alpha F_{\rm c} = 1$, Eq. (6) is plotted in Fig. 1a. At Doppler shift $\tilde{w} = 0$, the emission region is located in the plane of the sky passing through the star, hence none of this emission is occulted. In contrast at $\tilde{w} = 1$, only the material receding at the terminal speed can produce this emission, which must originate from behind the star, so all of the emission appearing at maximum redshift is occulted. At intermediate Doppler shifts, there is a gradual change between these two extremes.

If occultation is assumed unimportant and Eq. (5) is applied to the profile of Eq. (6) to obtain $y(w)$, the following expression is derived:

$$y(w) = 4\alpha F_{\rm c} \left[\frac{3\pi}{16} - \frac{3}{8} \sin^{-1} w + \frac{1}{4} w \sqrt{1 - w^2} \left(\frac{3}{2} + w^2 \right) \right]. \tag{7}$$

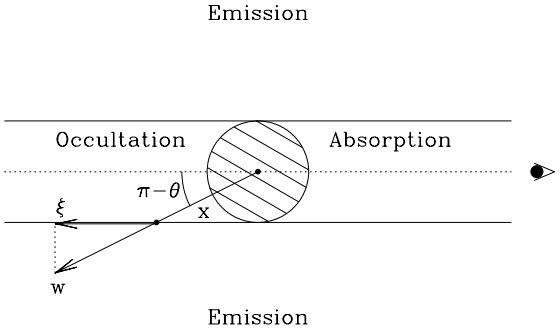

Fig. 2. Illustration of the geometry giving rise to the occultation. The observer is right. The speed ξ is the projection of $w(x)$ onto the stellar occulting tube, inside which no emission may be observed.

The velocity distribution of Eq. (7) is shown in Fig. 1b. Note that $w(y)$ deviates strongly from that of $w = 1$ and never even reaches $y = 1$. The reason for this failure to recover the correct constant velocity distribution is that the occultation of emitting material imposes a slope on the line profile that would not otherwise be there. We next derive an analytic solution to the case when occultation is included.

2.2. Inversion of a line profile including occultation

Fig. 2 illustrates the stellar wind geometry and shows the various regions giving rise to the emission, occultation, and absorption commonly observed in P Cygni profiles. The parameter ξ is the projection of the wind velocity onto the occulting tube and represents the maximal receding velocity that can be observed from a spherical shell of radius x expanding at $w(x)$. At any radius

$$\xi(x) = w(x)\sqrt{1 - \frac{1}{x^2}}, \tag{8}$$

where the factor $\sqrt{1 - 1/x^2}$ is the line-of-sight projection factor $\cos(\pi - \theta)$ as shown in Fig. 2.

The consequence of the occultation for the line profile is thus to replace Eq. (4) by

$$\Phi(\tilde{\xi}) = 1 + \frac{1}{4\alpha F_c} \int_{x_{\min}(\tilde{\xi})}^{\infty} \frac{dx}{x^2\, w^3(x)}, \tag{9}$$

which is valid for $\tilde{\xi} \geq 0$ (i.e., no absorption). Here $\tilde{\xi}$ is to ξ as $\tilde{w}$ is to w. Differentiating Eq. (9) gives the equality

$$x^2\, w^3\, \frac{d\xi}{dx} = \left[-4\alpha\, F_c \left(\frac{d\Phi}{d\tilde{\xi}}\right)_{\tilde{\xi}=\xi}\right]^{-1}. \tag{10}$$

Eliminating w in favor of ξ by using $w = \xi/\sqrt{1 - 1/x^2}$, and substituting $y = x^{-1}$ yields

$$\alpha\, F_c\, \frac{d\Phi}{d\xi}\, d\xi^4 = \left(1 - y^2\right)^{3/2}\, dy, \tag{11}$$

which may be integrated to obtain (replacing Eq. [5])

$$\alpha\, F_c \int_{\xi^4}^{1} \left(-\frac{d\Phi}{d\tilde{\xi}}\right) d\tilde{\xi}^4 = \frac{3}{8}\,\psi + \frac{1}{4}\,\sin 2\psi + \frac{1}{32}\,\sin 4\psi, \tag{12}$$

where $\psi = \sin^{-1} y(\xi)$. The RHS of Eq. (12) is monotonic in y and allows the recovery of $y(\xi)$ (and hence $y(w)$) from the occulted red-shifted emission. Under the assumptions of an optically thin line produced in a spherical wind, Eq. (12) is an *exact* relation for the profile inversion in the case of stellar occultation.

Note that the LHS of Eq. (12) is determined by the profile data; the value of ψ on the RHS must then be found from numerical root finding techniques. Denoting $h(\psi) = \frac{3}{8}\,\psi + \frac{1}{4}\,\sin 2\psi + \frac{1}{32}\,\sin 4\psi$, we plot $h(\psi)$ versus ψ in Fig. 3. For small ψ, the distribution $h(\psi)$ is nearly linear, but as ψ nears the value of $\frac{\pi}{2}$, the distribution becomes considerably flattened. It is worth noting that at these values of ψ, the root finding technique will require stringent tolerances to achieve a good estimate of $y(\xi)$, for which $\xi \approx 0$ and $y \approx 1$. The precision with which w is recovered for y near unity (i.e., the innermost regions of the wind) will be sensitive to numerical errors associated with root finding in this flattened region of the $h(\psi)$ distribution, because $w(y) = \xi/\sqrt{1 - y^2}$. This problem with the flatness of $h(\psi)$ is similar to that in curve-of-growth theory in the "log" part of the distribution: small errors in the line equivalent width transform to significant errors in the column density.

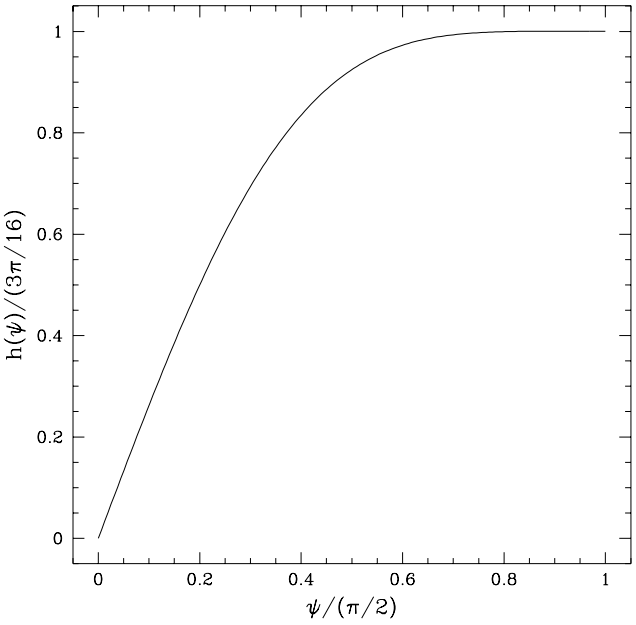

Fig. 3. Plot of $h(\psi)$ required to solve for $y(w)$. Note the considerable flatness of the distribution toward values of ψ near $\pi/2$.

Although this numerical problem will always be present in the line inversion, other effects may dominate the errors in the recovery of $w(y)$ from real line profiles, such as noise in the signal, profile sampling, or departures from our basic physical assumptions. The consequences of noise in the profile were briefly considered in BRCI and deserve a more thorough study in a separate work. The breakdown of our basic assumptions are investigated to some extent in the following section, where we apply the profile inversion to model lines.

3. Applications to model profiles

3.1. Considerations of the profile inversion approach

Before discussing results from the profile inversion, several issues must first be addressed: (1) how the parameter α is computed, (2) the numerical technique by which the integral of Eq. (12) is evaluated, and (3) the reliability of the results from the inversion. Regarding the first point, α is found by Eq. (3), if R, $\dot{M}_e$, D, $f_0(T)$, and v_∞ are known. However, in Eq. (12), there is a boundary condition that can be imposed, namely that $y = 1$ at $\xi = 0$ (i.e., $x = 1$ at the lower boundary of the wind at the stellar limb). Applying this boundary condition, the value of α can be determined empirically from the profile inversion itself. Setting $\psi = \pi/2$ in Eq. (12) and solving for α gives

$$\alpha = \frac{3\pi}{16 F_c} \left(\int_0^1 -\frac{d\Phi}{d\tilde{\xi}}\, d\tilde{\xi}^4\right)^{-1}, \tag{13}$$

where the integral proceeds over the entire red-shifted emission profile. Determining α in this way is the natural approach when dealing with real observations.

Even so, care must be taken with this approach, as several effects occurring toward low velocity shifts in the profile can systematically alter the empirically determined value of α. These effects include the presence of an underlying photospheric profile, broadening mechanisms other than thermal broadening and the bulk wind flow (e.g., stellar rotation, turbulence, Zeeman effect, Stark broadening), and optically thick line formation. In each of these cases, one should bear in mind the following two points.

(a) The consequences of these additional effects can significantly alter the profile structure, but will generally be limited toward line center. Naturally, our method is not likely applicable in cases where rotational and other non-thermal broadening mechanisms are a significant fraction of v_∞, nor in cases where the line formation is dominantly optically thick. Most of these "line core" effects will be relegated to the inner 100–200 km s^{-1} of the profile, or less in some cases (e.g., slow rotators, etc). We expect our inversion technique to have general applicability toward the line wings, where optical thinness is realized; however, if any of the line core effects described above are significant, the evaluation of α from the profile integration will be highly suspect.

(b) The mention of α leads to the second point. The value of α comes from an integral of the profile slope as *weighted* by the function $\tilde{\xi}^3$. Although the profile slope will be growing rapidly with decreasing velocity shift, the weighting factor is also dropping rapidly. Depending on the actual velocity distribution, the value of α may be more sensitive to either the wings or the line core, but it will not in general be completely determined by the profile shape near line center. Hence the effects described in (a), although potentially significant, need not always drastically bias the evaluation of α. An assessment of the line core effects must be made before applying our method. In favorable cases our method will yield valuable information on $v(r)$ that may be used as a guide for modelling line profiles from winds where more complicated processes are operating.

If α can be reliably determined, the fact that α is calculated empirically and that F_c is measured implies that we may solve for one of the intrinsic properties of the star which are related to α through expression (3), recalling that the basic scaling of α is

$$\alpha \sim \frac{D^2\, R\, v_\infty^3}{\dot{M}_e^2\, f_0(T)}. \tag{14}$$

Eq. (14) may be modified to eliminate the distance dependence by multiplying both sides of the expression by the continuum flux F_c. Assuming a blackbody stellar spectrum with

$$F_c D^2 = \pi B_\lambda(T) R^2, \tag{15}$$

the scaling of αF_c becomes

$$\alpha F_c \sim \frac{B_\lambda(T)\, R^3\, v_\infty^3}{\dot{M}_e^2\, f_0(T)}. \tag{16}$$

For the inversion of model profiles, Eq. (16) is used to estimate stellar radii directly from the model line profiles and to compare the estimates to the model inputs. A more general discussion of deriving stellar and wind parameters using the observed line profile is given in Sect. 4.

The second point to consider in applying the inversion technique is the numerical method used to evaluate Eq. (12). To obtain $y(\xi)$ or α requires the integration of a numerically computed derivative of real data. In terms of signal-to-noise, the inversion will be more stable owing to the integration over the differentiated data. However, it is not clear how the errors in the data will propagate.

An alternative approach is to consider a rearrangement of Eq. (12):

$$\int_{\xi^4}^1 \left(-\frac{d\Phi}{d\tilde{\xi}}\right) d\tilde{\xi}^4 = 4 \int_1^{\Phi(\tilde{\xi}=\xi)} \tilde{\xi}^3\, d\Phi. \tag{17}$$

Conceptually, one advantage to the RHS of this equation is the interpretation of the inversion as a weighted integration across the line profile, in which the integration begins at the greatest redshift in the line wing. Thus, particular line features, with appropriate weighting according to position in the profile, appear directly in the solution for the recovered distribution $w(y)$. Inspection of the RHS further suggests that if the wavelength calibration is highly accurate (typical of modern techniques), then $\tilde{\xi}$ will be well-determined, and the dominant source of error in the recovery of $v(r)$ will reside with the measured signal Φ in a linear way.

Lastly, having estimated α and inverted the line profile to obtain $w(y)$, there is a consistency check that may be applied to determine how well the inversion method is working. This check comes from a consideration of the line half equivalent width, HEW (i.e., the equivalent width of the emission from the occulted hemisphere only). Taking the HEW avoids having to consider the effects of absorption that are important for the full equivalent width of the line. For a spherical wind with occultation, the half equivalent width associated with the receding hemisphere can be derived as

$$\mathrm{HEW} = \frac{\lambda_0\, v_\infty}{c} \int_0^1 [\Phi(\tilde{\xi}) - 1]\, d\tilde{\xi} \tag{18}$$

$$= \frac{\lambda_0\, v_\infty}{4c\,\alpha\, F_c} \int_0^1 \frac{(1-y^2)^{3/2}}{\xi^2(y)}\, dy. \tag{19}$$

For $\xi(y)$ known from the profile inversion, and HEW measured, α can be found and compared to that from the profile inversion. The comparison of α from the profile inversion to that from the HEW provides a measure of confidence in the estimate of whatever parameter (e.g., R) is being evaluated from the value of α.

3.2. Model profile results: Assessment of the inversion technique

In this section the inversion technique of Eq. (12) that is based on an optically thin recombination line treatment and includes

occultation is applied to model wind profiles, first from a code that computes only optically thin profiles and second from a radiative transfer code that generates profiles based on the Sobolev approximation. Our motivation is to demonstrate that the inversion method is capable of recovering wind velocity distributions from simulated profiles where the input $v(r)$ is known, thereby allowing an assessment of the method's reliability.

In the first case, a numerical scheme was constructed to calculate emission line profiles for the redshifted side of P Cygni lines. The code assumes optical thinness, hence there is no radiative transfer, but the code does account for occultation. The inversion technique of expression (12) is therefore tested in cases where our assumptions are explicitly valid. Fig. 4 shows three columns for the redshifted line profile, the velocity distribution from the profile inversion as compared to the model input, and the difference between the recovered and input velocities. The model profiles of the first column have arbitrarily been normalized to a peak value of 0.1 and offset by a value of unity, so as to simulate an optically thin line superposed on a continuum.

The three profiles are for three different velocity distributions. The top profile is one that was calculated using a standard β-velocity law

$$v(r) = v_0 + (v_\infty - v_0)\left(1 - \frac{R}{r}\right)^\beta , \qquad (20)$$

with $\beta = 1$ and $v_0/v_\infty = 0.1$. The profiles in the middle and lower panels were computed from a more sophisticated velocity distribution according to

$$v(r) =$$

$$0.5\left[1 + \frac{2}{\pi}\tan^{-1}\left(\frac{r/R - 2}{\delta}\right)\right]\left[0.1 + 0.9\left(1 - \frac{R}{r}\right)\right] +$$

$$0.5\left[1 + \frac{2}{\pi}\tan^{-1}\left(\frac{2 - r/R}{\delta}\right)\right]\left[0.1 + 0.9\left(1 - \frac{R}{r}\right)^2\right] . \qquad (21)$$

This velocity law represents a combination of two β-laws with $\beta = 1$ and $\beta = 2$. At the radius $r/R = 2$, the arctangent function effects a switch between the $\beta = 2$ law for $r/R < 2$ and the $\beta = 1$ law for radii $r/R > 2$. The parameter δ controls how sharply the switch between the two β-laws will occur, with smaller values of δ resulting in more rapid transitions. Values of $\delta = 1.0$ and 0.1 were used in the calculation of the profiles, as indicated in Fig. 4.

In the middle column, the velocities $w(y)$ and $\xi(y)$ from the profile inversion are plotted as solid, and the model velocity profiles are shown as dotted. The $w(y)$ distributions always lie above those of $\xi(y)$. The recovered and model velocity distributions lie so close that it is often hard to distinguish between them. The difference in the velocity distributions, ΔVelocity, is shown in the rightmost column, which gives $\xi - \xi_{\rm mod}$ as solid and $w - w_{\rm mod}$ as dashed. The error in the recoveries are generally quite small except near $y = 1$. The jump present in the recovered w results from the root finding problem in the flat part of the $h(\psi)$ distribution, that was discussed in Sect. 2.2

Table 1. Stellar and model parameters

Star	ζ Pup	κ Cas	55 Cyg	HD4841
Sp. Type	O4f	B1Ia	B3Ia	B5Ia
$\log L$	6.02	5.5	4.94	5.18
$R/R_\odot$	17	43	37	69
$M/M_\odot$	60	35	15	15
$T_{\rm eff}$ (K)	45000	21000	16000	13700
$\log \dot{M}$	-5.18	-5.9	-6.88	-6.77
v_∞	2650	1650	600	450
$W^a_{\rm meas}(\mathrm{H}_\alpha)$	-3.6	-2.1	-0.1	-0.3
$W^a_{\rm LTE}(\mathrm{H}_\alpha)$	-5.0	-1.5	-0.11	-0.26
$W^a_{\rm NLTE}(\mathrm{H}_\alpha)$	+1.0	-0.3	-0.14	-0.22
β	1	2	2	3
v_0/v_∞	0.05	0.07	0.3	0.2

[a] A negative equivalent width indicates a line in emission; positive is for absorption.

Overall, the application of the profile inversion to pure optically thin lines does an excellent job of recovering the model input velocity distribution. It is worth noting the slight trough appearing in the ΔVelocity plot for the $\delta = 0.1$ profile. This low value of δ produces a sharp and nearly vertical jump in the model velocity distribution. The frequency gridding of the line profile was not sufficient for the inversion technique to fully resolve the sudden transition between the $\beta = 2$ and $\beta = 1$ velocity laws. Thus, the profile inversion will fail to recover details of the true monotonic $v(r)$ in real stellar winds if the velocity structure is not reflected in the observed profile. One reason for this failure is the problem of insufficient frequency resolution, as just discussed. A second possibility that could arise in real winds is that although resolved, some velocity structures may not have sufficient emission to significantly alter the profile, for example a sudden increase of the wind speed at large radius. Although these limitations should be noted, the fact that some detailed features of $v(r)$ may not be recovered suggests that the inversion method is not inhibited from obtaining the gross properties of the wind velocity distribution.

Next the inversion method was applied to emission lines as generated by the NLTE code of Cassinelli et al. (1978). This radiative transfer code computes H_α line profiles using the Sobolev method. Note that the calculations include only thermal broadening and have no photospheric absorption component. We further note that the Sobolev method is known to fail when the wind flow velocity is of order the wind sound speed, but alterations to the emission profile under such conditions will appear near line center where other difficulties already discussed will also be encountered and may be of greater significance.

Parameters were chosen to typify four stars with different spectral types as listed in Table 1. These parameters were taken to be representative of real stars and selected to sample several different spectral types and wind velocity parameters. The β-law form of Eq. (20) was adopted once again.

Note that the observed H_α equivalent widths, taken from Leitherer (1988), are also listed in Table 1. The ratios v_0/v_∞ and the β values were chosen to produce roughly similar equiv-

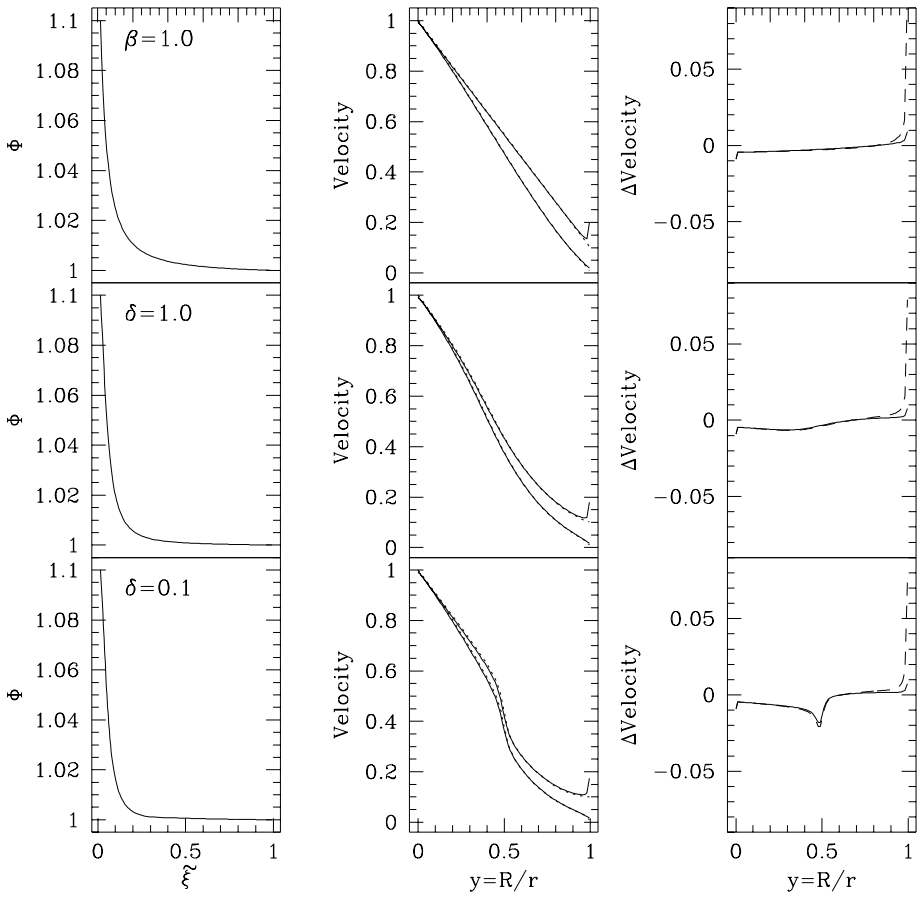

Fig. 4. The profile inversion as applied to three explicitly optically thin lines generated from three different $w(x)$ laws (see text). The emission profiles in the red wing (including occultation) are shown in the left column. The recovered distributions $w(y)$ (upper solid) and $\xi(y)$ (lower solid) are plotted with the model input distributions (dotted) in the middle column. The right column shows the difference between the recovered and model velocity distributions, with $w - w_{\rm mod}$ dashed and $\xi - \xi_{\rm mod}$ solid.

alent widths in the model profiles while providing a variety of wind velocity distributions to test the inversion technique. However, these simulations are for purposes of demonstration only and should not be considered as actual determinations of the velocity distribution in the winds of these specific stars, for we are actually inverting model profiles and not real data.

Fig. 5 shows the application of the inversion technique to several LTE H_α profiles in the same format as that of Fig. 4. The four rows are for the different star types as labeled; the three columns are for the H_α profile (left), the model and recovered velocity laws (middle), and the difference between the model and recovered velocity laws (right).

Note that we assume an isothermal wind with temperature $T = T_{\rm eff}$ of the star and that the source function in the stellar photosphere and in the wind is Planckian at $T_{\rm eff}$. The consequence is that none of the profiles show absorption below the continuum level. This follows for lines in LTE from the argument that if (a) the line is optically thin, one observes the stellar photosphere with $B_\lambda(T_{\rm eff})$ and (b) if the line is quite optically thick, the photospheric continuum is completely attenuated, so that one observes the wind emission also with $B_\lambda(T_{\rm eff})$. Hence, there can be no net absorption. In the future it may be possible to drop the isothermal assumption by considering multiline observations, a topic to be considered elsewhere.

Returning to the middle column of Fig. 5, both the recovered and model velocity distributions $\xi(y)$ and $w(y)$ are plotted just as in Fig. 4. (For comparison $\xi(x)$ and $w(x)$ are plotted in Fig. 6.) As indicated in the right column of Fig. 5, the recovery of the velocity distribution tends to be quite good for $y \lesssim 0.9$ (or $x \gtrsim 1.1$), giving $\xi - \xi_{\rm mod}$ and $w - w_{\rm mod}$ typically less than about 0.04, corresponding to fractional errors of less than about 5%. The ΔVelocity plots for the B3Ia and B5Ia stars show a short vertical line segment at $y = 0$. In the case of these stars, the emission line is so optically thin that numerical round-off yields zero line flux at the extreme wings, hence y remains constant for these first few points, accounting for the presence of the vertical segments.

Fig. 7 shows profiles and the results of the inversion technique for the cases of Fig. 5, but with the NLTE effects included. The profiles of Fig. 7 are "mildly" NLTE, with departure coefficients b_3 of about 2 asymptotically in the different models. The effect of NLTE populations relative to LTE for the line emission is twofold: the absorption in the blue wing is more significant, and the emission in the red wing is enhanced. The full equivalent width of the line may increase or decrease, but the HEW of the red wing increases in all four cases (c.f., Table 2). Although the results of the profile inversion in the NLTE case is somewhat poorer than for the LTE lines, the technique still does quite well in recovering both $\xi(y)$ and $w(y)$ in all four of our examples. The stellar radius is consistently underestimated in the NLTE case owing to the enhanced emission in the red wing leading to smaller values of α and thus reduced estimates of R.

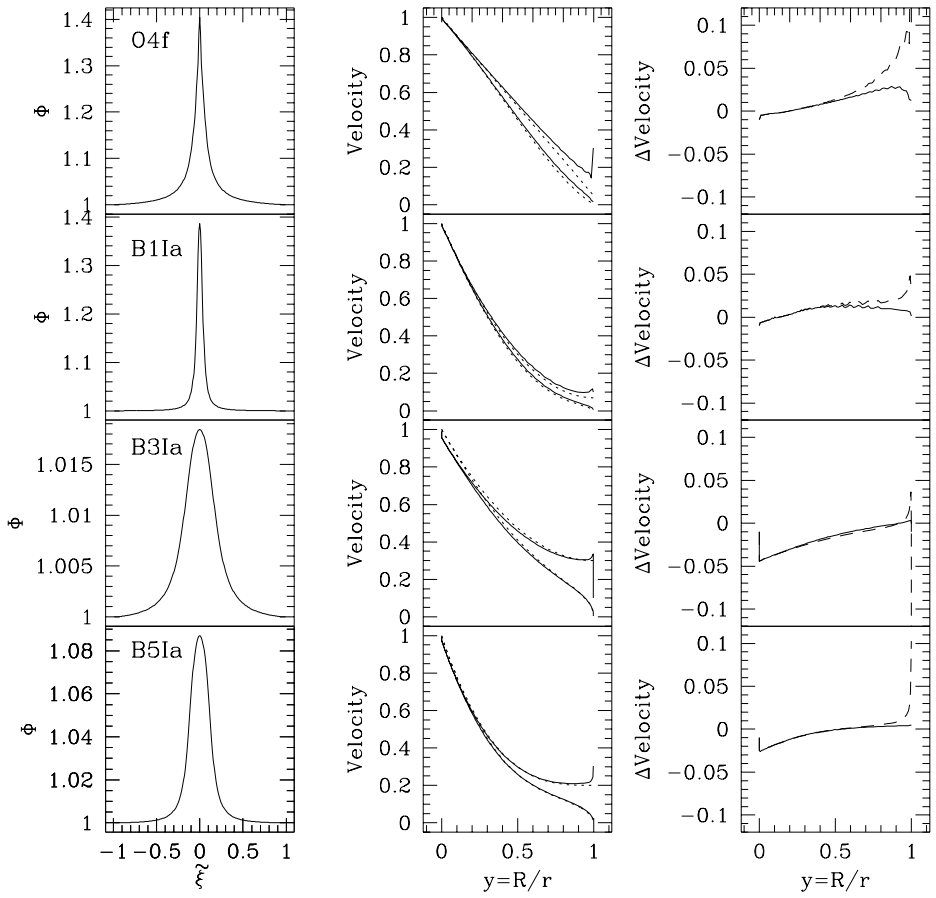

Fig. 5. The results for the line inversion recovery of $w(y)$ as applied to four synthetic LTE profiles. A label with the spectral type of the model star is given to distinguish the different line profiles.

Table 2. Results for the inversion of model line profiles

Star	ζ Pup	κ Cas	55 Cyg	HD4841
LTE $(\alpha F_c)_{inv}$	28.5	211.1	216.9	158.5
LTE $(\alpha F_c)_{HEW}$	29.1	183.8	206.5	159.3
NLTE $(\alpha F_c)_{inv}$	18.6	148.3	152.3	121.8
NLTE $(\alpha F_c)_{HEW}$	18.9	131.4	146.7	122.1
LTE R_{inv}/R_{mod}	0.96	0.96	1.01	0.97
LTE R_{HEW}/R_{mod}	0.97	0.92	0.99	0.97
NLTE R_{inv}/R_{mod}	0.84	0.85	0.89	0.89
NLTE R_{HEW}/R_{mod}	0.84	0.82	0.88	0.89

The success in matching $w(y)$ even in the NLTE case results from determining α directly from the profile itself. In the NLTE case, the α of Eq. (3) would be proportional to b_3, so that the value of α as computed directly from the profile includes the effect of the NLTE populations, even though we assume that b_3 = 1 in our theory. Thus, the chief discrepancy in the recovery of $w(y)$ between the NLTE and LTE cases comes from our failure to include $b_3(y)$ in the integral of Eq. (9). It should be noted that in applications to real hydrogen recombination lines, the NLTE effects in B star winds can be sensitive to both spectral type and mass-loss rate, but less so in O stars. So, for hydrogen lines from B stars, some additional care is required in interpreting results from using the profile inversion under the current assumptions.

For both the LTE and NLTE cases, we have estimated the stellar radii from the value of αF_c taken from the profiles, with the results listed in Table 2. To estimate the stellar radii, it was required to know the function $f_0(T)$. In the general NLTE case, this function is derived analytically by equating $j = f_0(T) n_e^2$ to $hcA_{32}n_3b_3/\lambda_0$ and using the Saha-Boltzmann equation, giving

$$f_0(T) = \frac{h\,c\,A_{32}\,g_3\,b_3}{\lambda_0\,u_e(T)}\,e^{\chi_{3,\infty}/kT}, \qquad (22)$$

where g_u is the statistical weight of the upper level u, $u_e(T)$ is the partition function of a free electron, and $\chi_{3,\infty}$ is the ionization potential of hydrogen from the u = 3 level. Note that this derivation of f_0 is valid only for a pure hydrogen wind that is almost completely ionized.

In estimating stellar radii from the model results, LTE is assumed in our inversion method, hence b_3 = 1. Table 2 gives stellar radii as determined from both the profile inversion and also from the HEW. Comparing the predictions for the photospheric radii, the LTE cases clearly give more accurate estimates than do the NLTE cases, with the NLTE cases underestimating R by a factor of about $b_3^{1/3}$. However, the superiority of the inversion method as compared to the HEW computation for predicting R is not so evident. In practice, we recommend employing the

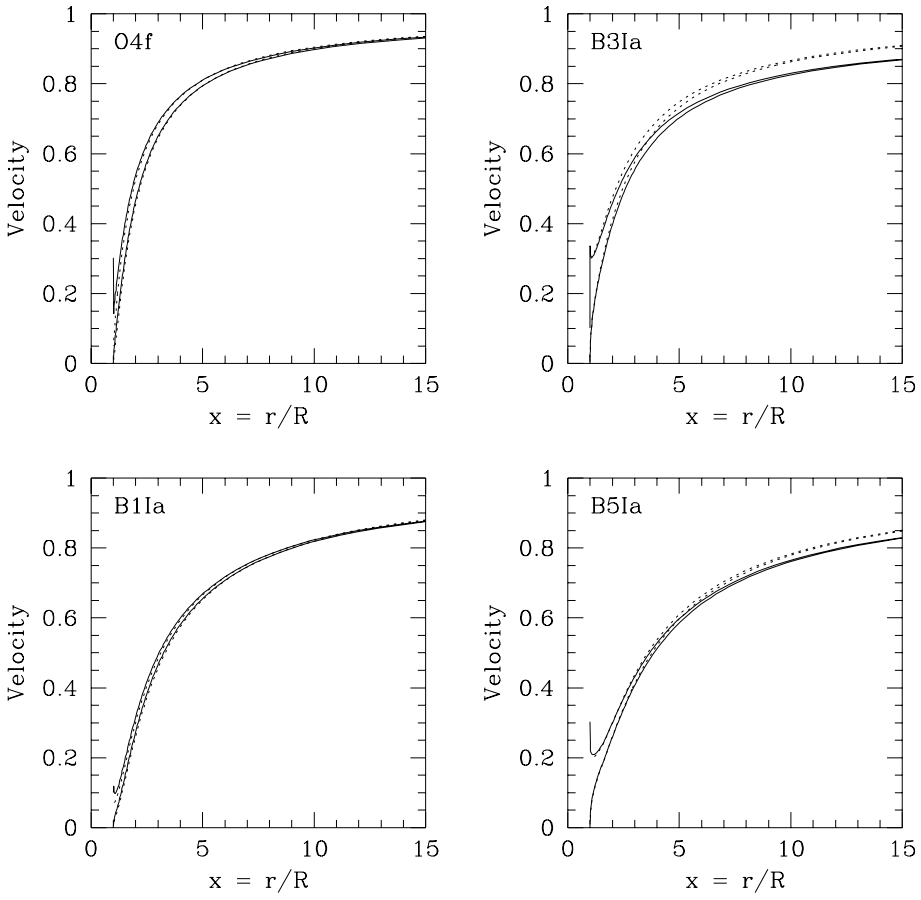

Fig. 6. The velocity distributions ξ and w from the middle column of Fig. 5, now plotted against $x = r/R$ instead of y. The results of the profile inversion are shown as solid and the model input as dotted.

inversion method to fix α and the HEW method as a consistency check, because the $\xi(y)$ distribution used to compute the theoretical HEW must come from the profile inversion itself. Significant discrepancies could signify errors in the numerical analysis or sensitivities to the profile's characteristics, such as poor signal-to-noise or poor sampling of the profile.

4. Determination of intrinsic stellar parameters

Our inversion technique for deriving the wind velocity distribution requires a coefficient that depends on several parameters intrinsic to the star or the wind, such as $\dot{M}_e$, R, D, v_∞, and T. Of these, the terminal speed is usually the easiest to measure, and for this discussion v_∞ is taken as known. Further assuming that the stellar temperature can be estimated, a procedure for inferring the wind mass-loss, photospheric radius, and stellar distance using our inversion method is outlined as follows.

To begin, recall that for a recombination line, the α parameter relates to the wind and line properties as

$$\alpha = \frac{8\pi^2\, D^2\, \lambda_0\, m_H^2\, R\, v_\infty^3}{f_0(T)\, \dot{M}_e^2\, c}. \tag{23}$$

Since α is independently measured from the recombination line, Eq. (23) provides the first constraint for determining the three unknowns $\dot{M}_e$, R, and D. Two more constraints are required.

Consider a resonance line, for which the dependence of α on the stellar and wind parameters is different from that of the recombination line. In this case the emissivity, $j'(r)$, for an optically thin line whose upper state population is governed by the incident stellar radiation field is (see Appendix A.)

$$j'(r) = K'(r,T)\, W(r)\, n_e(r), \tag{24}$$

where the dilution factor $W = \frac{1}{2}\,(1 - \sqrt{1 - R^2/r^2})$ and (in standard notation) an expression for $K'(r,T)$ is given by

$$K'(r,T) = 4\pi B_\lambda(\lambda_1, T)\, \frac{\pi e^2}{m_e c}\, \frac{gf}{g_u}\, \frac{n_u}{n_e}\, \left(\frac{b_l}{b_u}\, e^{h\nu_1/kT} - 1\right). \tag{25}$$

Note that λ_0 was used to specify the wavelength of the recombination line, and here λ_1 is chosen for the wavelength of the resonance line. The ratio of the population density in the atom's upper level to that of the electron density is

$$\frac{n_u}{n_e} = \gamma_u\, q_i\, A_E\, \mu_e\, X, \tag{26}$$

where $\gamma_u = n_u/n_i$ is the fraction of the ion's number density in the upper level u, $q_i = n_i/n_E$ is the ionization fraction of the ion species, $A_E = n_E/n_H$ is the elemental abundance of the species relative to hydrogen, X is the mass fraction of hydrogen, and μ_e is the mean molecular weight per free electron. For this discussion we take the function $K'(r,T)$ as constant throughout

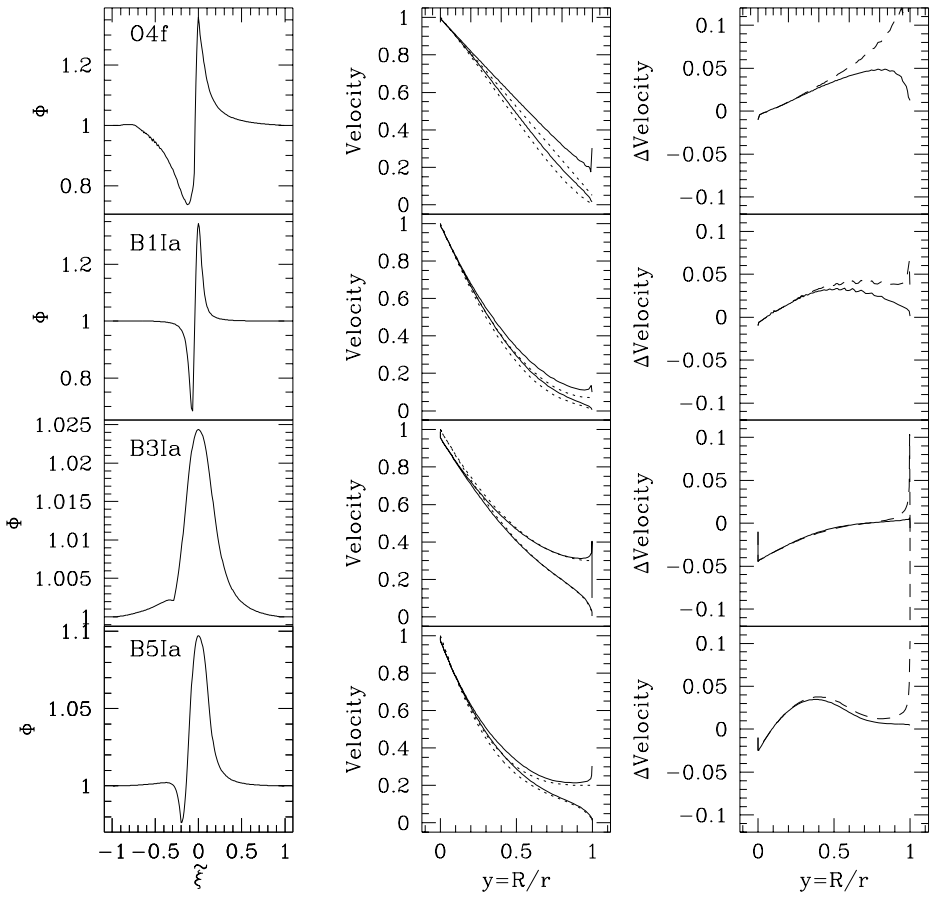

Fig. 7. The same as Fig. 5 but for the case of NLTE line profiles.

the wind, but in general $K'(r,T)$ will vary with radius (see Appendix A). The derivation could be generalized to more realistic cases if the ionization distributions of the ions were known, but it is in fact the run of ionization fractions throughout the wind that typically constitute the greatest uncertainty in the spectroscopic analysis of stellar winds. We pursue the special case of $K'(r,T)$ equals a constant $K(T)$ to demonstrate how recombination and resonance profiles may be used to infer the intrinsic stellar properties using our inversion technique.

The profile analysis for a resonance line proceeds exactly as that for a recombination line but with j' of Eq. (24) substituted for j in Eq. (1). An expression for the resonance line emission similar to that of Eq. (2) for a recombination line is given by

$$F_\lambda(\tilde{w}) = \frac{1}{3\,\alpha'} \int_{x_{\rm min}(\tilde{w})}^{\infty} \frac{W(x)\,dx}{x^2\,w^2(x)}. \tag{27}$$

The parameter α' for the case of a resonance line is

$$\alpha' = \frac{8\pi\,D^2\,\lambda_1\,m_{\rm H}\,v_\infty^2}{3\,K(T)\,\dot{M}_{\rm e}\,c\,R}\,, \tag{28}$$

which now provides a second constraint for determining $\dot{M}_{\rm e}$, R, and D.

A third constraint is still required to solve for all three of these parameters. We have already used such a constraint in the previous section. Namely, if the underlying intrinsic flux distribution of the continuum emission can be assumed or modelled from theory, then the ratio D/R can be related to the ratio of intrinsic flux to measured flux. For example, assuming a blackbody continuum spectrum at the wavelength of the line in consideration, we eliminate the distance dependence in α and α' to obtain the expressions

$$\alpha\,F_{\rm c} \;=\; \frac{8\pi^3\,B_\lambda(\lambda_0,T)\,m_{\rm H}^2\,\lambda_0\,R^3\,v_\infty^3}{f_0(T)\,\dot{M}_{\rm e}^2\,c}\,, \tag{29}$$

$$\alpha' F_{\rm c} \;=\; \frac{8\pi^2\,B_\lambda(\lambda_1,T)\,m_{\rm H}\,\lambda_1\,R\,v_\infty^2}{3K(T)\,\dot{M}_{\rm e}\,c}\,. \tag{30}$$

Eqs. (29) and (30) can be used to derive $\dot{M}_{\rm e}$ and R, and thereby to obtain D by employing Eq. (15).

The following system of scaling relations result:

$$\dot{M}_{\rm e} \;\sim\; \frac{\alpha F_{\rm c}}{(\alpha' F_{\rm c})^3}\,, \tag{31}$$

$$R \;\sim\; \frac{\alpha F_{\rm c}}{(\alpha' F_{\rm c})^2}\,, \tag{32}$$

$$F_{\rm c}\,D^2 \;\sim\; R^2 \sim \frac{(\alpha F_{\rm c})^2}{(\alpha' F_{\rm c})^4}\,. \tag{33}$$

Thus, for known stellar temperature T, terminal speed v_∞, and continuum spectrum (e.g., blackbody), we have shown how $\dot{M}_e$, R, and D may be derived from the profile inversions of one recombination line and one resonance line, because the inversions provide α and α'. Eqs. (31)–(33) were derived under rather restrictive simplifications but do indicate the important information that may potentially be obtained from the results of the profile inversion.

An interesting aspect of our discussion is the definition of the radius R to be that of the photosphere. It is common to define the photospheric radius as the distance from the star where the optical depth in the continuum, τ_c, is about unity along the line-of-sight joining the observer and the star's center. In the case of low mass-loss winds such as those of OB stars, the photosphere typically coincides with the radius at the base of the wind where the flow speed is subsonic. However, in the case of massive stellar winds such as those of Wolf-Rayet stars, the photospheric radius can occur in the bulk wind flow. Hence, our inversion technique can be used to infer the approximately hydrostatic stellar radius for optically thin winds with $\tau_c \lesssim 1$ or the continuum formation radius in optically thick winds with $\tau_c \gtrsim 1$.

In the case of the Wolf-Rayet winds, the dominant continuous opacity at the radio and infrared wavelengths is that of free-free, so that the photospheric radius grows with increasing wavelength (Wright & Barlow 1975). The analysis of a sequence of wind lines could place strong constraints on the wind velocity distribution because (a) the inversion of each individual profile provides $v(r)$ exterior to the photospheric radius at the wavelength of the line and (b) the inferred photospheric radius can be related to the expansion of the photosphere from a consideration of the continuum emission. In fact, the combination of points (a) and (b) permits an alternative approach to deriving $v(r)$ from an inversion analysis of multiline observations, *even if* the velocity distribution is non-monotonic. One drawback of this approach is that the radius of continuum formation for any one line is not known in absolute terms, but only relative to radii inferred from other lines. However, the slope of the continuum emission provides another essential ingredient for recovering $R(\lambda)$ in absolute terms. The topics of total line intensity distributions and non-monotonic wind velocity laws will be explored further in a separate paper.

5. Summary and discussion

This paper has explored an inversion technique for recovering wind velocity distributions, taking into account the effects of stellar occultation. For optically thin lines formed in spherical winds, the inversion method accurately reproduces the velocity law in model profiles to quite small radii, typically to $r/R \gtrsim 1.1$, even in the case of NLTE profiles. The failure of the method to recover $w(x)$ closer to the photosphere is related to numerical difficulties in the root finding scheme, but this problem arises only very near $r/R = 1$. The inversion method therefore shows promise as a diagnostic of stellar wind velocity structures.

Furthermore, an algorithm has been proposed whereby quantities intrinsic to the star and wind, such as $\dot{M}_e$, R, and D, may be derived if two different line profiles can be obtained: one a recombination line and the other a resonance line. Applications of this algorithm are limited owing to the simplifying assumptions adopted in Sect. 4, but the method shows potential for using profile inversion to derive important fundamental parameters.

Aside from the assumptions of optical thinness and sphericity, our profile inversion approach has also assumed isothermality and LTE level populations. In general, temperature variations throughout the wind and NLTE departure coefficients that depend on radius should be expected. It may be possible to extract these distributions from the profiles by considering several lines, but such a study is beyond the scope of this paper.

We stress that the inferred value of R refers to the radius of the continuum formation. The distinction here is that in massive winds, such as those of Wolf-Rayet stars, the effective photosphere occurs in the outflow itself, thus our method allows for its determination as a function of wavelength using multiline observations. In such cases alternative approaches to inverting the data for inferring the wind properties are being considered. These new approaches, involving such things as the distributions of the line equivalent widths and the continuum slope, will be the subject of a future paper.

Acknowledgements. We wish to thank J. Puls for several helpful comments that have improved this paper. This work was supported by a UK PPARC Rolling Grant and a NATO Research Collaboration Grant. Cassinelli acknowledges partial support from NSF grant #9417186.

Appendix A: the inversion technique as applied to resonance lines

Here an analytic expression for the line profile inversion of an optically thin resonance line formed in a spherically symmetric stellar wind is derived. We begin with Eq. (1):

$$F_\lambda(\Delta\lambda) = \frac{c}{2\lambda_1 D^2} \int_{r_{\rm min}}^{\infty} \frac{j'(r)\, r^2}{v(r)}\, dr, \tag{A1}$$

where j' for the case of a resonance line is used in distinction to j for a recombination line. To derive j', we employ the well-known Sobolev theory for an optically thin line (c.f., Mihalas 1978). The intensity along a ray passing through the emitting volume is given by

$$I_\lambda = \int S_\lambda\, e^{-\tau_\lambda}\, d\tau_\lambda. \tag{A2}$$

For $\tau_\lambda \ll 1$, the source function $S_\lambda \approx I^*_\lambda\, \beta_c/\beta = W(r) I^*_\lambda$, where β_c and β are the penetration and escape probabilities, thus

$$I_\lambda \approx \int W(r)\, I^*_\lambda\, k(r)\, \Psi_\lambda\, dz, \tag{A3}$$

where we have substituted

$$d\tau_\lambda = k(r)\, \Psi_\lambda\, dz, \tag{A4}$$

with k the opacity coefficient, Ψ_λ the normalized emission profile taken to be a delta-function at a Doppler shift in the line, and dz the differential path length along the ray.

However, the intensity is also given by

$$I_\lambda = \frac{1}{4\pi} \int j'(r)\, \Psi_\lambda \, dz, \tag{A5}$$

where j' has units Wm^{-3}. Hence we infer that

$$j'(r) = W(r)\, I^*_\lambda \, k(r) = K'(r,T)\, W(r)\, n_\mathrm{e}(r). \tag{A6}$$

By inspection the constant $K'(r,T)$ is

$$K'(r,T) = \frac{4\pi\, I^*_\lambda \, k}{n_\mathrm{e}} =$$

$$4\pi B_\lambda(T)\, \frac{\pi\, e^2}{m_\mathrm{e}\, c}\, \frac{gf}{g_\mathrm{u}}\, \frac{n_\mathrm{u}}{n_\mathrm{e}} \left(\frac{b_l}{b_\mathrm{u}}\, e^{h\nu_1/kT} - 1 \right), \tag{A7}$$

where $I^*_\lambda = B_\lambda(\lambda_1, T)$ was assumed. The ratio $n_\mathrm{u}/n_\mathrm{e}$ depends on various factors involving the level excitation and the species ionization, so is in general a function of radius. We parametrize $K'(r = Rx, T) = K(T)\, x^\delta\, w^\nu\, W^\gamma$, where the power law indices δ, ν, and γ are constants and of course $w = w(x)$ and $W = W(x)$.

Analogous to Eq. (9), the normalized wind-broadened line profile valid for $\tilde{\xi} \geq 0$ is

$$\Phi(\tilde{\xi}) = 1 + \frac{c}{2\lambda_1\, D^2\, F_\mathrm{c}} \int \frac{j'(r)\, r^2}{v(r)}\, dr \tag{A8}$$

$$= 1 + \frac{c}{2\lambda_1\, D^2\, F_\mathrm{c}} \int \frac{K'(r,T)\, W(r)\, n_\mathrm{e}(r)\, r^2}{v(r)} dr \tag{A9}$$

$$= 1 + \frac{1}{3\alpha' F_\mathrm{c}} \int_{x_\mathrm{min}}^{\infty} \frac{W^{1+\gamma}\, dx}{x^{2-\delta}\, w^{2-\nu}}, \tag{A10}$$

where the substitution $x = r/R$ was made in the last line. As in Eq. (26), the uncertainty regarding the ionization distribution throughout the wind is sufficiently poor that we simply take $\delta = \nu = \gamma = 0$, implying $K'(r,T) = K(T)$ only. Then the relation between α' and the physical parameters of the wind and the line emission is given in Eq. (28). Differentiating $\Phi(\tilde{\xi})$ by $\tilde{\xi}$ for this particular special case gives the relation

$$\frac{w^2(x)}{W(x)}\, \frac{d\xi}{dx} = \left[-3\alpha'\, F_\mathrm{c} \left(\frac{d\Phi}{d\tilde{\xi}} \right)_{\tilde{\xi}=\xi} \right]^{-1}. \tag{A11}$$

Making a change of variable $x = y^{-1}$ and substituting $w(y) = \xi(y)/\sqrt{1-y^2}$ yields

$$3\alpha'\, F_\mathrm{c}\, \tilde{\xi}^2 \left(\frac{d\Phi}{d\tilde{\xi}} \right)_{\tilde{\xi}=\xi} d\tilde{\xi} = \frac{1}{2}(1-y^2) \left[1 - \sqrt{1-y^2} \right] dy. \tag{A12}$$

Integrating this last expression gives the solution

$$\alpha' F_\mathrm{c} \int_{\xi^3}^{1} \left(-\frac{d\Phi}{d\tilde{\xi}} \right) d\tilde{\xi}^3$$

$$= \frac{1}{2} \int_0^y \left[(1-y^2) - (1-y^2)^{3/2} \right] dy \tag{A13}$$

$$= \frac{1}{6} y\,(3-y^2) - \frac{1}{2} \left(\frac{3}{8}\, \psi + \frac{1}{4}\, \sin 2\psi + \frac{1}{32}\, \sin 4\psi \right) \tag{A14}$$

where $\psi = \sin^{-1} y$. Note that in the solution (A14) for an optically thin resonance line, the second parenthesis is in fact the solution for a recombination line (c.f., Eq. [12]). In the case that δ, ν, and γ are nonzero but integers, analytic solutions may often still be derived for Eq. (A10).

Applying the boundary condition that $y = 1$ when integrating over the line profile from $\tilde{\xi} = 0$ to 1 allows for the determination of α' analogous to that of α. The exact expression is

$$\alpha' F_\mathrm{c} = \frac{1}{2} \left(\frac{2}{3} - \frac{3\pi}{16} \right) \left[\int_0^1 \left(-\frac{d\Phi}{d\tilde{\xi}} \right) d\tilde{\xi}^3 \right]^{-1}. \tag{A15}$$

The constant coefficient has an approximate value of 0.0388. The empirical evaluation of α' can be used to infer intrinsic stellar and wind parameters as discussed in Sect. 4.

References

Beals C. S., 1929, MNRAS 90, 202
Brown J. C., Richardson L. L., Cassinelli J. P., Ignace R. (BRCI), 1997, A&A, 325, 677
Cassinelli J. P., Olson G. L., Stalio R., 1978, ApJ 220, 573
Castor J. I., Abbott D. C., Klein R. I., 1975, ApJ 195, 157
Chandrasekhar S., 1934, MNRAS 94, 522
Friend D. B., Abbott D. C., 1986, ApJ 311, 701
Groenewegen M. A. T. Lamers H. J. G. L. M., 1989, A&AS 79, 359
Lamers H. J. G. L. M., Leitherer C., 1993, ApJ 412, 771
Lamers H. J. G. L. M., Cerruti-Sola M., Perinotto M., 1987, ApJ 314, 726
Leitherer C., 1988, ApJ 326, 356
Lucy L. B., Solomon P. M., 1970, ApJ 159, 879
Menzel D. H., 1929, PASP 41, 344
Mihalas D., 1978, Stellar Atmospheres (Freeman: New York)
Pauldrach A., Puls J., Kudritzki, R. P., 1986, A&A 164, 86
Puls, J., Kudritzki, R.-P., Herrero, A., et al., 1996, A&A 305, 171
Wright A. E., Barlow M. J., 1975, MNRAS 170, 41

This article was processed by the author using Springer-Verlag LaTeX A&A style file *L-AA* version 3.